Earth and Space Science

RESEARCH ARTICLE
10.1029/2022EA002481

Special Section:
Twenty Years of Observations from the Atmospheric Infrared Sounder

The Earth-Observing Aqua Satellite Mission: 20 Years and Counting

Claire L. Parkinson[1]

[1]Cryospheric Sciences Laboratory, NASA Goddard Space Flight Center, Greenbelt, MD, USA

Abstract The Earth-observing Aqua spacecraft was launched on 4 May 2002 and has now completed 20 years of collecting and transmitting data regarding the Earth's radiation budget, atmosphere, oceans, land, and ice. Although launched with a design life of 6 years, four of its instruments continue to operate and provide high-quality data streams more than 20 years after launch. The Aqua data are readily available to users worldwide and have been used in thousands of scientific publications and in numerous practical applications, including weather forecasting, air-quality assessments, and monitoring of forest fires, dust storms, volcanic ash plumes, oil spills, and crop yields.

Key Points:

- The Aqua satellite has collected 20 years of data on the Earth's radiation budget, atmosphere, oceans, land, and ice
- Aqua data have been used in thousands of scientific publications presenting details and insights about the Earth system and changes in it
- Aqua data have also been used in numerous practical applications, from weather forecasting to monitoring forest fires and crop yields

Correspondence to:
C. L. Parkinson,
Claire.L.Parkinson@nasa.gov

Citation:
Parkinson, C. L. (2022). The Earth-observing Aqua satellite mission: 20 years and counting. *Earth and Space Science*, *9*, e2022EA002481. https://doi.org/10.1029/2022EA002481

Received 29 JUN 2022
Accepted 31 AUG 2022

Author Contributions:
Conceptualization: Claire L. Parkinson
Writing – original draft: Claire L. Parkinson
Writing – review & editing: Claire L. Parkinson

1. Introduction

The National Aeronautics and Space Administration's (NASA's) Aqua spacecraft was launched on 4 May 2002, with a design life of 6 years. It has now been in orbit for 20 years, during which time it has orbited the Earth over 106,000 times and collected data that have been used in over 20,000 scientific publications and in numerous practical applications.

For most of its first 20 years after launch, Aqua has been in a carefully controlled sun-synchronous orbit at an altitude of ~705 km, orbiting the Earth every 98.8 min and crossing the equator going north at approximately 1:35 p.m. local time and going south at approximately 1:35 a.m. local time. Throughout these 20 years on orbit, Aqua has been collecting and transmitting data on the Earth's radiation budget, atmosphere, oceans, land, and ice.

The data collected by the Aqua Earth-observing instruments during an orbit are stored temporarily in Aqua's onboard solid state recorder (SSR) and downlinked to ground stations in Alaska and/or Norway's Svalbard island complex as Aqua passes over the north polar region. This results in a science data flow of ~88 Gbytes per day transmitted to the level 0 processing facility at NASA's Goddard Space Flight Center (GSFC), from where they are transmitted to various data processing facilities, which typically receive the data between 30 min and 2 hr after the data were collected. Aqua also transmits real-time data through direct broadcast continuously throughout an orbit, except during the periods of downlink from the SSR. The direct broadcast data are available to anyone with an appropriate antenna and are estimated to be captured and processed by over 200 ground stations worldwide. This allows immediate use of local data, which can be particularly important in times of disasters such as forest fires.

This article provides a summary of the Aqua Earth-observing instruments, a brief history of Aqua from launch through its first 20 years on-orbit, and an overview and sample highlights of the science and practical applications benefiting from the Aqua data.

2. The Aqua Earth-Observing Instruments

Aqua carries on board six Earth-observing instruments: the Atmospheric Infrared Sounder (AIRS), the Advanced Microwave Sounding Unit (AMSU), the Humidity Sounder for Brazil (HSB), the Advanced Microwave Scanning Radiometer for the Earth Observing System (EOS) (AMSR-E), the Clouds and the Earth's Radiant Energy System (CERES; two copies), and the Moderate Resolution Imaging Spectroradiometer (MODIS) (Figure 1). The three sounders (AIRS, AMSU, and HSB) combine to form a powerful sounding system centered on the AIRS instrument, and this sounding system has a single AIRS/AMSU/HSB Science Team, generally referred to as the AIRS Science Team, covering all three instruments. Separate science teams exist for each of the CERES, MODIS, and AMSR-E instruments.

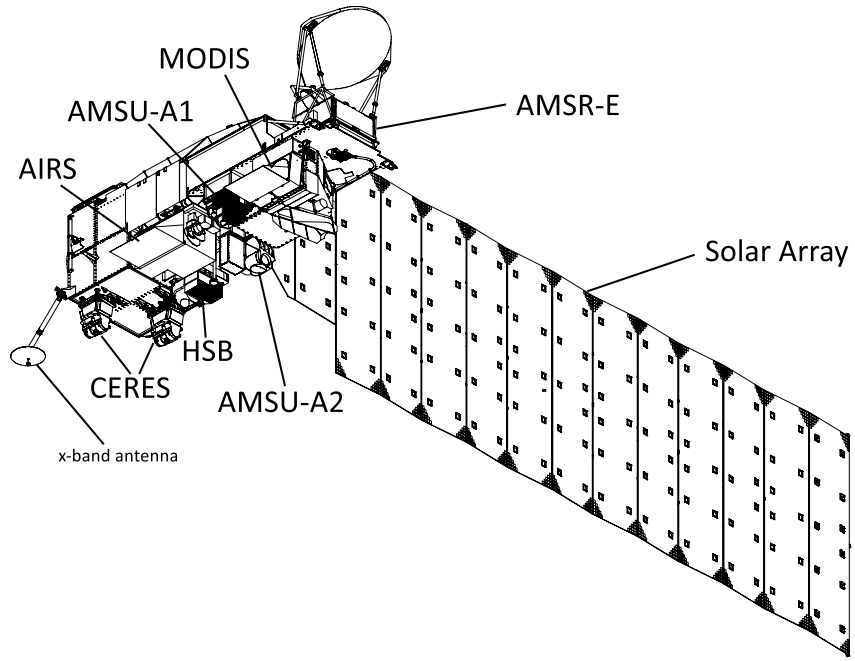

Figure 1. Schematic of the Aqua spacecraft, its six Earth-observing instruments, 12-panel solar array, and x-band antenna. The solar array extends 14 m and provides solar energy to the spacecraft battery and instruments. Advanced Microwave Sounding Unit (AMSU)-A1 and AMSU-A2 are the two physically unconnected components of the AMSU instrument. (Line drawing courtesy of Aqua's spacecraft company Northrop Grumman [formerly TRW], with labels added.)

AIRS is the one Earth-observing instrument that is fully unique to Aqua. It is a 2,382-channel grating spectrometer with 2,378 channels measuring infrared radiation at a spatial resolution of 13.5 km at nadir and four channels measuring visible/near-infrared radiation at a spatial resolution of 2.3 km at nadir. AIRS provides vertical profiles of atmospheric temperature and water vapor, plus measurements of atmospheric carbon dioxide, methane, ozone, and sulfur dioxide and various cloud and surface parameters. When built, it was a major technological advance over all previous space-based spectrometers, which typically had 15–20 detectors measuring broad bands of infrared radiation. AIRS instead has 2,378 infrared detectors, each measuring a specific wavelength and transmitting close to 3 million measurements a day. Furthermore, each AIRS detector has a redundant backup, in case the primary detector fails, and the detectors are maintained at a stable temperature through an innovative cryocooler, resulting in the high level of stability that enables AIRS data to be used to accurately determine signals of climate change. More information on the AIRS instrument can be found in Aumann et al. (2003) and in Pagano et al. (2022), the latter also including the technology efforts aimed at the next generation of grating spectrometer infrared sounders.

AMSU is a 15-channel sounder measuring microwave radiation at 23–90 GHz (0.3–1.3 cm) with a spatial resolution of 40.5 km at nadir. It is identical to AMSU-A instruments that have flown on a series of National Oceanic and Atmospheric Administration (NOAA) satellites since 1998. AMSU provides temperature profiles from the surface to an altitude of 40 km, along with information on cloud liquid water. It also facilitates cloud clearing of AIRS observations and allows for enhanced AIRS retrievals in partially cloudy scenes. More information on the AMSU instrument can be found in Mo (1996) and in Lambrigtsen (2003).

HSB is a 4-channel sounder measuring microwave radiation at 150–190 GHz (0.16–0.20 cm) with a spatial resolution of 13.5 km at nadir. It is identical to the AMSU-B instruments that have flown on a series of NOAA satellites since 1998, and it was provided to the Aqua program by Brazil's Instituto Nacional de Pesquisas Espaciais (INPE, Brazil's National Institute for Space Research). Until HSB ceased operating in 2003, the HSB data were used to detect high levels of precipitation and to derive atmospheric humidity profiles and cloud liquid water profiles. More information on the HSB instrument can be found in Lambrigtsen (2003) and in Lambrigtsen and Calheiros (2003).

AMSR-E is a 12-channel passive microwave radiometer measuring microwave radiation at 6.9–89 GHz, with spatial resolutions ranging from 6 × 4 km for the 89 GHz measurements to 74 × 43 km for the 6.9 GHz measurements. AMSR-E was provided by Japan's National Space Development Agency (NASDA; later merged into the Japan Aerospace Exploration Agency (JAXA)). AMSR-E is no longer operating but was a tremendous success in collecting 9 years of data (its design life had been 3 years) on a wide variety of atmospheric and surface variables, followed by intercalibrations with Japan's follow-on AMSR2 instrument on its Global Change Observation Mission-Water (GCOM-W) satellite. AMSR-E data allowed the derivation of rainfall rates, oceanic surface wind speeds, integrated water vapor and cloud water amounts, sea surface temperatures (SSTs), sea ice coverage and characteristics, snow water content, and soil surface wetness. Because of measuring at microwave rather than visible wavelengths, the data on surface variables were obtained during darkness as well as daylight and under most weather conditions, including the presence of nonprecipitating clouds. More information on the AMSR-E instrument can be found in Kawanishi et al. (2003). HSB and AMSR-E are the two non-U.S. Earth-observing instruments on Aqua. AIRS, AMSU, CERES, and MODIS were all provided by NASA.

CERES is a 3-channel scanning radiometer measuring radiation from 0.3 μm to >100 μm, with a spatial resolution of 20 km at nadir. One channel measures reflected shortwave radiation, one measures total outgoing radiation, and one measures the outgoing radiation in the 8–12 μm atmospheric window. Aqua has two CERES instruments, flight model (FM)-3 and FM-4. The first CERES instrument, a proto flight model, was launched on 27 November 1997 on the tropical rainfall measuring mission (TRMM) and is no longer operating. The next two CERES, FM-1 and FM-2, were launched on 18 December 1999 on the Terra satellite and are still operating; and CERES instruments also fly on the Suomi National Polar-Orbiting Partnership (NPP) satellite and the NOAA-20 satellite. The central purpose of each CERES instrument is to collect data on the Earth's radiation budget. Each CERES instrument can operate in a cross-track scanning mode or in a rotating azimuth plane mode, with the cross-track scanning providing long-term Earth radiation budget measurements and the rotating azimuth plane scanning providing additional angular radiance information, leading to improved accuracy in the data products. More information on the CERES instrument can be found in Wielicki et al. (1996).

MODIS is a 36-band cross-track scanning radiometer measuring visible and infrared radiation in the range 0.4–14.5 μm, with data product spatial resolutions ranging from 250 m to 1 km. The Aqua MODIS is the second of two MODIS instruments, the first having been launched on 18 December 1999 on the Terra satellite. MODIS measures a wide variety of atmosphere, ocean, and land variables, including cloud optical depth, cloud particle size, water vapor, aerosols, atmospheric temperature, SST, ocean color, sea ice coverage, land cover type, net primary productivity, leaf area index, and snow cover. Having MODIS on both Aqua and Terra has allowed these measurements to be made under both morning and afternoon conditions, as Terra's sun-synchronous orbit has had Terra crossing the equator for most of the past 20 years at approximately 10:30 a.m. and 10:30 p.m. local time, complementing Aqua's early morning and early afternoon crossing times. More information on the MODIS instrument can be found in Barnes et al. (1998) and in Xiong and Barnes (2006).

3. A Brief History of Aqua From Launch Through Its First 20 Years on-Orbit

The Aqua satellite was launched into space from Vandenberg Air Force Base, 15 km northwest of Lompoc, California, in the early morning of 4 May 2002, promptly at the start of its 10-min 2:55–3:05 a.m. (local California time) launch window. The spacecraft was carried into orbit on board a Delta II rocket, the bulk of which dropped into the Pacific, as planned, shortly after launch. The rocket's second stage propelled Aqua from California south across the Pacific, over Antarctica, and north to Africa, with spacecraft separation from the rocket's second stage occurring over Africa (in view of NASA's Malindi tracking station in Kenya) at 59 min 30 s after launch. Twelve and a half minutes later, as Aqua flew over northern Europe, its solar array was unfurled in view of the Svalbard tracking station. With the successful unfurling of the solar array, which provides solar power to the spacecraft and its on-board instruments, control of the spacecraft shifted from Mission Control at Vandenberg to Earth Science Mission Operations (ESMO) at NASA Goddard Space Flight Center in Greenbelt, Maryland.

Following launch, each of the Earth-observing instruments was turned on and checked out before beginning its Earth-observing role (Table 1). The one major issue that arose during the check-out of the instruments came when the initial data were returned from AMSR-E on 24 May 2002. These data were clearly flawed, but within days the Japanese AMSR-E experts determined the cause of the problem and provided ESMO with corrective instructions to relay to the spacecraft and AMSR-E. The flaws in the data were thereby removed, allowing a high-quality "first

Table 1
Dates for the Powering on of Each of the Aqua Earth-Observing Instruments, for the First Light Images for Each Instrument, and, in the Cases of the Two Instruments That Are no Longer Operating, for the End Date of Science-Quality Data Collection, Plus References for the Instrument Details

Instrument	Powered on	First light	End date	References for instrument details
AIRS	5/6/2002	6/14/2002	Ongoing	Aumann et al. (2003); Pagano et al. (2022)
AMSR-E	5/4/2002	6/4/2002	10/4/2011	Kawanishi et al. (2003)
AMSU	5/12/2002	6/14/2002	Ongoing	Mo (1996); Lambrigtsen (2003)
CERES FM-3	5/7/2002	6/22/2002	Ongoing	Wielicki et al. (1996)
CERES FM-4	5/7/2002	6/22/2002	Ongoing	Wielicki et al. (1996)
HSB	5/14/2002	6/14/2002	2/5/2003	Lambrigtsen (2003); Lambrigtsen and Calheiros (2003)
MODIS	5/24/2002	6/24/2002	Ongoing	Barnes et al. (1998); Xiong and Barnes (2006)

Note. AIRS, Atmospheric Infrared Sounder; AMSR-E, Advanced Microwave Scanning Radiometer for the Earth Observing System; AMSU, Advanced Microwave Sounding Unit; CERES, Clouds and the Earth's Radiant Energy System; HSB, Humidity Sounder for Brazil; MODIS, Moderate Resolution Imaging Spectroradiometer.

light" image to be produced from AMSR-E on 4 June 2002, averaging data from 2 to 4 June 2002. By the end of June 2002, all six of Aqua's Earth-observing instruments were returning high-quality data streams. The remaining full checkout of all the spacecraft subsystems was declared complete on 1 September 2002, 120 days after launch.

On 5 February 2003, the Aqua mission suffered its first major loss, when the HSB instrument ceased to operate due to a scan mirror motor failure. Although disappointing, the loss of HSB was not devastating to the mission because the AIRS Science Team had been well aware of the possibility that the HSB and AMSU sounders might fail before AIRS and were well on the way to developing algorithms to ensure that the core AIRS data products could continue to be produced even in the face of the loss of one or both of the HSB and AMSU instruments. Once the HSB failed, the AIRS/AMSU/HSB algorithms were replaced by AIRS/AMSU algorithms.

A much lesser problem occurred on 30 March 2005, when the shortwave channel on the CERES FM-4 failed. Prior to 30 March 2005, typically one of the two CERES on Aqua would be operating in its cross-track mode, collecting data for long-term Earth radiation budget measurements, while the other Aqua CERES would be operating in its rotating azimuth plane mode, collecting angular radiance data. The angular radiance data were needed for creating CERES angular distribution models (ADMs), and the record until 30 March 2005 provided sufficient data for the ADMs, making the rotating azimuth plane operations no longer essential. Both CERES on Aqua could then be operated in the cross-track mode, with all three channels of FM-3 and two of the three channels of FM-4 continuing to collect high-quality data.

On 1 September 2008, 6 years after the end of its 120-day checkout period, Aqua completed its 6-year "prime" mission and entered into its "extended" mission, that is, extended beyond the 6-year design life. On 2 December 2008, Aqua's end-of-prime-mission review was successfully held, establishing that Aqua had fulfilled each of its 10 Mission Success Criteria and thereby was declared a success. The 10 Mission Success Criteria were:

1. Produce the first high-spectral-resolution global infrared spectra of the Earth. [Accomplished with AIRS data]
2. Obtain a highly accurate temperature profile of the troposphere. [Accomplished with AIRS data; Figure 2]
3. Extend the improved TRMM rainfall characterization to the extra tropics. [Accomplished with AMSR-E data; Figure 3]
4. Produce the first global SST daily maps under nearly all sky conditions for a minimum of 1 year. [Accomplished with AMSR-E data]
5. Produce large-scale global soil moisture distributions for regions with low vegetation. [Accomplished with AMSR-E data]
6. Produce calibrated global observations of the Earth's continents and ocean surfaces. [Accomplished with MODIS data]
7. Capture and document two seasonal cycles of terrestrial and marine ecosystems and atmospheric and cloud properties. [Accomplished with MODIS data]
8. Produce two seasonal/annual Earth radiation budget records. [Accomplished with CERES data]
9. Produce improved measurements of the diurnal cycle of radiation by combining Aqua and Terra measurements. [Accomplished with CERES data]

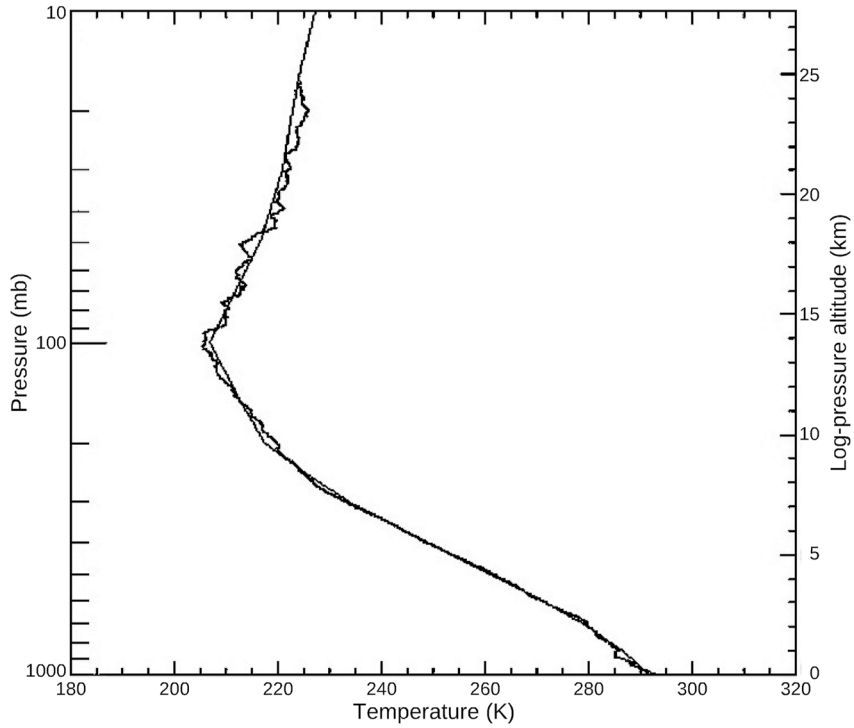

Figure 2. AIRS temperature profile over Chesapeake Bay (smooth curve) juxtaposed with a radiosonde profile (more jagged curve), for 13 September 2002. (Plot from Wallace McMillan of the AIRS Science Team, with relabeling.)

10. Produce combined cloud property and radiation balance data to allow improved studies of the role of clouds in the climate system. [Accomplished with CERES and MODIS data]

After a highly successful 9 years of data collection, AMSR-E suffered a major anomaly on 4 October 2011, ending its science data collection. The instrument was restarted on 4 December 2012, but attempts to return it to its fully operational rotation rate of 40 revolutions per minute (rpm) failed, preventing it from resuming its earlier science-level data collection. Still, it successfully operated at 2 rpm for the next 3 years, and this allowed AMSR-E to provide valuable cross-calibration data for JAXA's follow-on AMSR2 instrument launched on 18 May 2012, on Japan's GCOM-W satellite. AMSR-E transitioned to survival mode on 9 December 2015 and was powered off on 3 March 2016.

On 20 February 2021, Aqua reached the milestone of having completed 100,000 orbits of the Earth. By this time, Aqua was running out of fuel, and decisions had to be made regarding how best to allot the remaining fuel. Fuel is used for maneuvering the spacecraft, for instance to avoid space debris and to maintain tight control over the spacecraft's orbit. When launched, Aqua carried 225 kg of fuel. For Aqua's first 19 years on orbit, this fuel supply allowed ESMO to maintain Aqua in a tightly controlled sun-synchronous orbit at an altitude of approximately 705 km, with equatorial crossing times (mean local times (MLTs)) of 1:30–1:36 p.m. when going north across the equator and 1:30–1:36 a.m. when going south. This was done through orbit-controlling maneuvers of the spacecraft several times a year. By the end of 2021, less than 30 kg of fuel remained, and the decision was made to cease further orbit-controlling maneuvers, reserving the remaining fuel for debris avoidance maneuvers and, eventually, orbit-lowering and end-of-mission maneuvers. As a result, since January 2022, Aqua is operating in a free-drift mode, with its altitude slowly decreasing and the MLT of its observations slowly drifting to later times. Projections indicate that, if the mission continues to operate in its current free-drift mode, the MLT of the Aqua observations will drift from the 1:36 p.m. and 1:36 a.m. MLTs in January 2022 to approximately 3:50 p.m. and 3:50 a.m. MLTs in August 2026, when power generation limitations would likely end the science data collection.

The quality of the Aqua measurements is expected to remain high as the orbit drifts, although the impact of the drift on the Aqua data products will depend on the individual products and their uses, with, for instance, the altered illumination and viewing angles impacting the long-term consistency of the MODIS bidirectional

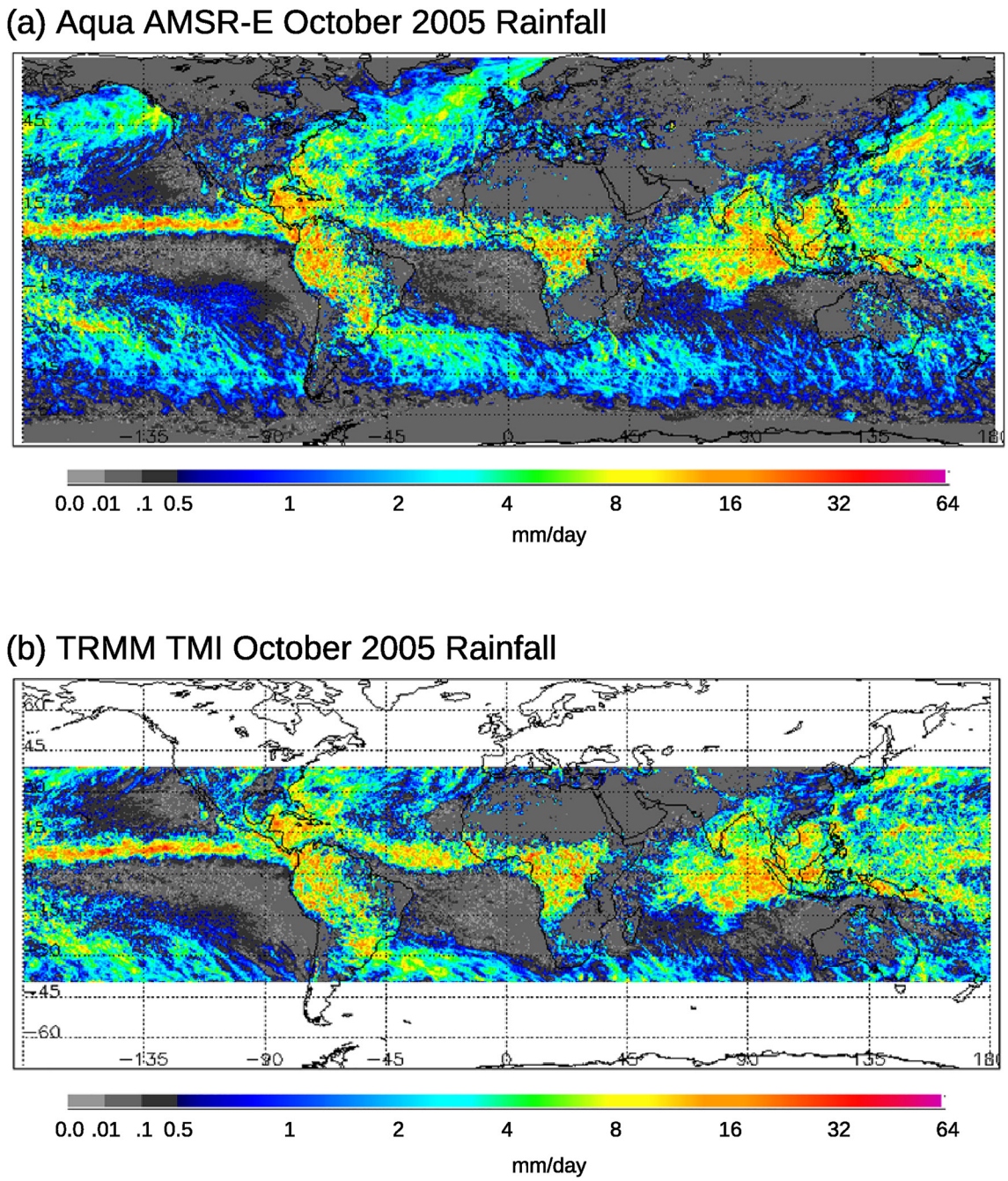

Figure 3. Globally mapped rainfall rates for October 2005, from Aqua Advanced Microwave Scanning Radiometer for the Earth Observing System (AMSR-E) data (top image) and from Tropical Rainfall Measuring Mission (TRMM) Microwave Imager (TMI) data (bottom image). (Images from Chris Kummerow and Ralph Ferraro of the AMSR-E Science Team.)

reflectance distribution function (BRDF) time series and the use of the BRDF in vegetation monitoring (e.g., see Petri and Galvao (2019) and Yan et al. (2022) for illumination and viewing angle complications for BRDF and vegetation monitoring). The drift could also lead to scheduling conflicts at the Aqua data downlink stations.

Although HSB and AMSR-E are the only two Aqua instruments that are no longer operating, there have been several instances, over the course of Aqua's 20 years on orbit, when one issue or another has arisen with the other instrumentation aboard the spacecraft. The two such anomalies that occurred most recently, in the first half of 2022, were a problem with the SSR on 22 February 2022, and a problem with the power controller for the

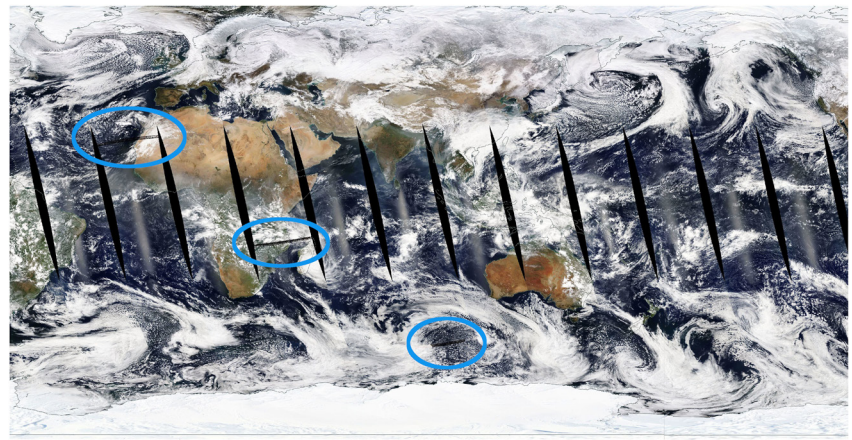

Figure 4. Aqua Moderate Resolution Imaging Spectroradiometer (MODIS) global image from 22 February 2022, highlighting (in blue ovals) the effects of the loss of approximately 19 s of MODIS data every two orbits. Black indicates missing data, and the close-to-horizontal black strips show the missing data from the 22 February 2022 solid state recorder anomaly. The larger, regularly spaced, closer-to-vertical slanted black strips show the missing data between the satellite orbits; the location of the slanted black strips shifts from day-to-day, so that averages over two or more days do not have such missing data. (Image from NASA WorldView, https://worldview.earthdata.nasa.gov, with ovals added.)

spacecraft's electrical subsystem on 31 March 2022. In both cases and all previous such cases, ESMO was able to resolve the problem and return the spacecraft to nominal operations. In the SSR case, the anomaly became apparent when approximately 19 s of corrupted AIRS and MODIS data were being transmitted every two orbits of the Earth (e.g., Figure 4). ESMO was able to determine that the corrupted data came from submodule 255 of the SSR, after which ESMO corrected the problem on 23 March 2002, by successfully instructing the spacecraft to no longer use submodule 255. The power controller (PC) anomaly occurred when there was an unexpected shift from the primary PC-A controller to the secondary PC-B controller. This anomaly is thought to have been a "single event upset" (SEU) and not likely to reoccur, which is fortunate as it resulted in the temporary cessation of data collection from all four still-operating Earth-observing instruments (AIRS, AMSU, CERES, and MODIS). After extensive troubleshooting, ESMO was able to determine that PC-A was still viable and successfully shifted the control back to PC-A on 13 April 2022, reestablishing nominal operations for all spacecraft and instrument functions by 16 April 2022.

As of 4 May 2022, the 20th anniversary of the launch of this satellite with a six-year design life, Aqua's AIRS, AMSU, CERES, and MODIS instruments are all continuing to collect high-quality science data.

4. Science Using Aqua Data

The Aqua data are freely available for use by scientists and others from around the world. Specifically, AIRS, AMSU, and HSB data are available from the Goddard Earth Sciences Data and Information Services Center (disc.gsfc.nasa.gov/AIRS), AMSR-E data and MODIS snow and ice data are available from the National Snow and Ice Data Center (nsidc.org/data/amsre and nsidc.org/data/modis, respectively), CERES data are available from the Langley Research Center (LaRC) Distributed Active Archive Center (DAAC) (eosweb.larc.nasa.gov), MODIS land data are available from the Land Processes DAAC (lpdaac.usgs.gov), MODIS atmosphere data are available from the Level 1 and Atmosphere Archive and Distributed System (ladsweb.nascom.nasa.gov), MODIS ocean color data are available from the Ocean Biology Processing Group (oceancolor.gsfc.nasa.gov), and MODIS SST data are available from the Physical Oceanography DAAC (podaac.jpl.nasa.gov/datasetlist?searchAQUA). The ready availability and high quality of these data have made them widely used by the science community, with over 20,000 papers incorporating Aqua data. This section provides an overview of how the data have been used, through a small but illustrative sampling.

4.1. Water Measurements From Aqua

"Aqua" being Latin for "water," the Aqua spacecraft was named for the large amount of information it reveals about water in the Earth system. This includes water in its liquid, solid, and gaseous forms, including liquid

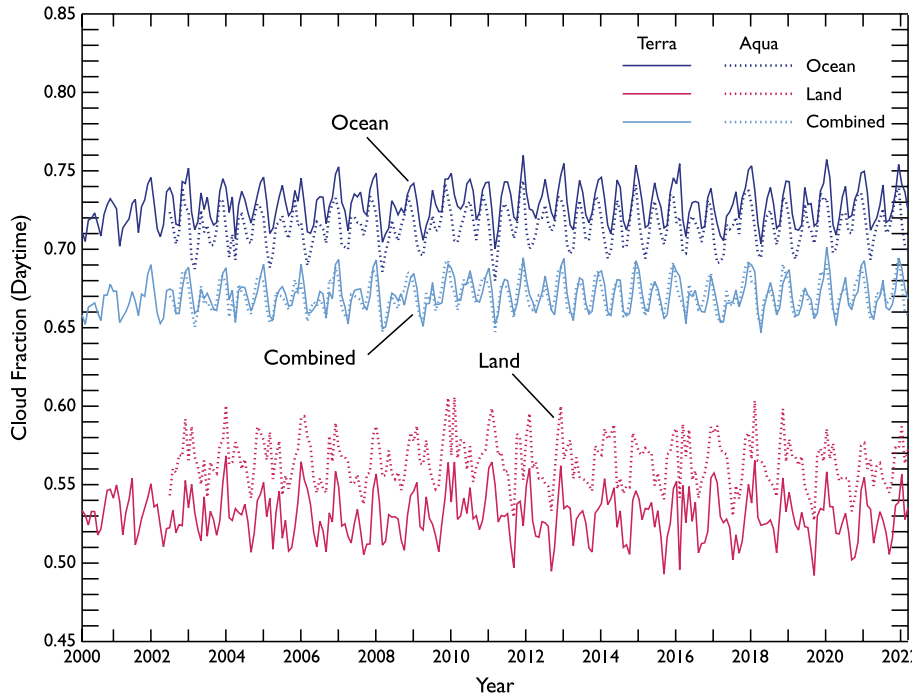

Figure 5. Global mean daytime cloud fraction, February 2000 to March 2022, from the Moderate Resolution Imaging Spectroradiometer (MODIS) instruments on Terra (solid curves) and Aqua (dotted curves), separated to global ocean coverage (black curves), global land coverage (red curves), and full global coverage, combining ocean and land (blue curves). (Plot from MODIS Science Team member Michael D. King, who created the figure from Level 3 data processed by Nandana Amarasinghe. The plot is updated from Figure 5 in King et al., 2013, through using Collection 6.1 rather than Collection 5 of the MODIS data sets and expanding the plot with an additional 9 years of data. The Terra time series begin in February 2000, marking the start of the Terra MODIS data set; the tick marks for the subsequent years, 2001–2022, are placed at the start of each year.)

ocean and lake water, solid ocean and lake water (i.e., sea ice, lake ice, and icebergs), atmospheric water vapor, atmospheric liquid and solid water (e.g., in clouds), precipitation, soil moisture, snow cover, and land-based ice.

Key components of the water cycle are all included in Aqua-derived data products. For instance, SSTs have been derived from both MODIS data (e.g., Kilpatrick et al., 2015) and AMSR-E data (e.g., Nielsen-Englyst et al., 2018), evaporation from AIRS data (e.g., Boisvert et al., 2020), evapotranspiration from MODIS data (e.g., Mu et al., 2011; Nishida et al., 2003), water vapor from AIRS data (e.g., Irion et al., 2018; Worden et al., 2019), precipitation from AMSR-E data (e.g., Joseph et al., 2009), and soil moisture from AMSR-E data (e.g., Bhagat, 2015; Jackson et al., 2009).

Cloud data from Aqua have received considerable research attention, in part due to the combined importance of clouds in the climate system and the uncertainties regarding their role in ongoing and predicted climate change. Cloud measurements from AIRS/AMSU and MODIS include cloud-top height, cloud-top temperature, cloud particle phase, cloud optical thickness, cloud effective radius, integrated water path, and fractional cloud cover (e.g., Naud & Kahn, 2015 for AIRS/AMSU data and Platnick, Meyer, et al., 2017 for MODIS data). A notable result, determined from Aqua and Terra MODIS data, is that clouds cover approximately 67% of the Earth at any time, in contrast to the 50% estimate that was common prior to the MODIS data (King et al., 2013) (Figure 5). AIRS data are allowing enhanced descriptions of cloud microphysics (Kahn et al., 2014), and AIRS and CERES data together have been used to determine the effects of cloud microphysics on outgoing longwave radiation (Huang et al., 2014). Similarly, MODIS and CERES data have been used to examine the radiative effects of different cloud regimes (Oreopoulos et al., 2016).

AMSR-E water measurements were incorporated with other satellite data to establish a global drying trend in soil moisture between 1988 and 2010 (Dorigo et al., 2012) and have also been used in flood analyses (e.g., Temimi et al., 2011), as have MODIS data (Fayne et al., 2017). The absence of water can be an even more serious problem

than excess water, and both the AIRS data and the MODIS data have proven valuable in the analyses and monitoring of drought conditions (e.g., Farahmand et al., 2015 using AIRS data; J. Zhang, Mu, & Huang, 2016 using MODIS data).

Aqua data have been used in numerous studies to examine interconnections involving water within the Earth system, including the use of AIRS data to examine the sensitivity of tropical deep convection events to SSTs (Wong & Teixeira, 2016), the use of CERES data to show that over the tropical oceans shortwave reflection by low clouds decreases when the ocean warms (Brient & Schneider, 2016), and the use of AIRS and AMSR-E data to quantify the increases in ocean to atmosphere moisture fluxes as Arctic sea ice decreases (Boisvert et al., 2013).

4.2. Climate Change Measurements From Aqua

The Aqua instruments measure far more than water, and among the most important groupings of its measurements are the measurements regarding climate change.

The CERES instruments measure outgoing radiation at the top of the atmosphere, categorized for Earth observations as both shortwave radiation (ultraviolet and visible) and longwave radiation (infrared and microwave). The CERES Science Team has compared the outgoing radiation measured by the CERES instruments on Aqua and Terra with the incoming radiation measured by the total irradiance monitor (TIM) on the Solar Radiation and Climate Experiment satellite to quantify the radiative imbalance at the top of the atmosphere, determining that for the period 2001–2010, the incoming radiation to the Earth exceeded the outgoing radiation by 0.50 ± 0.43 Wm^{-2} (Loeb et al., 2012).

It is widely thought that the radiative imbalance at the top of the atmosphere is caused at least in part by the increase in greenhouse gases in the Earth's atmosphere. The AIRS instrument not only obtains information on the Earth's most abundant greenhouse gas, water vapor, mentioned in the previous section, but also on the second and third most abundant greenhouse gases, carbon dioxide (CO_2) and methane (CH_4) (Figure 6), which are the greenhouse gases most discussed in the context of human-induced increases. In fact, the AIRS CO_2 product provided the first global daily CO_2 concentration maps and did so with an accuracy better than 2 parts per million by volume (ppmv) (Chahine et al., 2005, 2008). Calibration of the AIRS Pacific Ocean CO_2 data with the in situ measurements from Mauna Loa provides a close match for both the strong annual cycle and the upward trend in the CO_2 record (Strow & Hannon, 2008). Regarding methane, the AIRS data for the period 2003–2016 show that despite the latitudinal variation in atmospheric methane, with markedly more methane in the northern hemisphere than in the southern hemisphere, at every latitude the amount of atmospheric methane has increased (Zou et al., 2019).

Global warming is also well recorded in the AIRS data, as illustrated for the 2003–2017 period in Susskind et al. (2019). Comparison of the AIRS data with global records derived from in situ data sets shows a very close match in regions well covered by in situ data but greater differences in regions with limited in situ data, confirming that for global records, the satellite data are preferred (Susskind et al., 2019).

Among the expected consequences of warming is a reduction in sea ice, and sea ice reductions have indeed been recorded with AMSR-E and other data sets. CERES data have been used to estimate the increased solar radiative heating in the event of a total disappearance of Arctic sea ice throughout the sunlit portion of the year, finding that the effect would be equivalent to one trillion tons of CO_2 emissions (Pistone et al., 2019).

4.3. Air-Quality Measurements From Aqua

MODIS images of such phenomena as dust storms, fires, and volcanic eruptions provide striking depictions of instances of low air quality (e.g., Figure 7), and both MODIS and AIRS data have been used in assessing forest fire impacts on air quality (e.g., Adame et al., 2018; Field et al., 2016; Kim & Sarkar, 2017; Miller et al., 2011).

AIRS data are also used to monitor and assess aspects of air quality that are not directly visible, in particular through AIRS-derived data sets on carbon monoxide, ozone, and methane (e.g., Figure 8). Findings include a prominent decrease in northern hemisphere atmospheric carbon monoxide over the period 2002–2019 (Buchholz et al., 2021), an increase in atmospheric methane in India over the period 2003–2021 (Hari et al., 2022), and analyses of the transport of carbon monoxide and ozone pollutants across the Pacific from Asia to North America (Hsu et al., 2012; Huang et al., 2017; Lin et al., 2012).

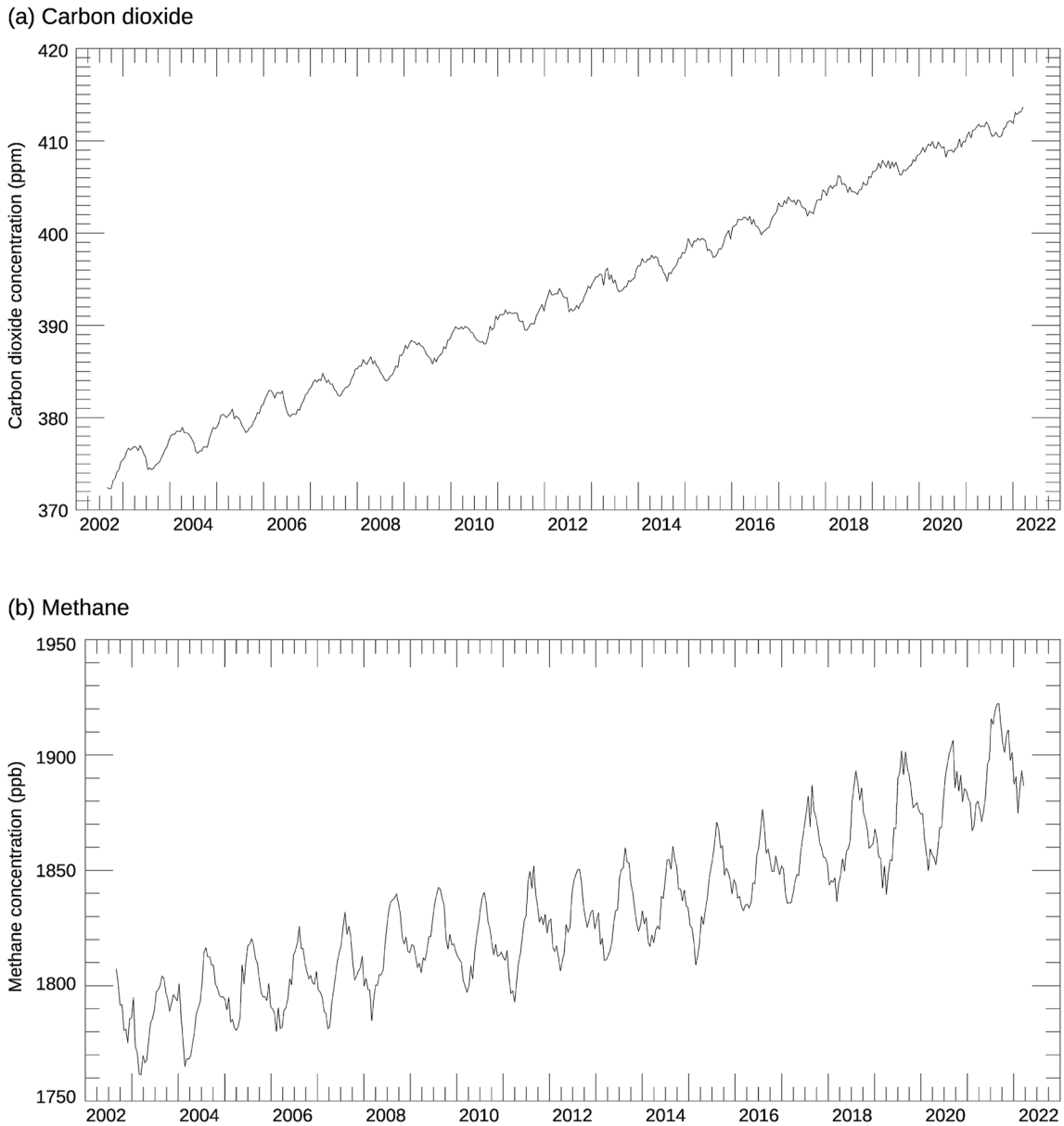

Figure 6. Selected time series of Atmospheric Infrared Sounder (AIRS) tropospheric greenhouse gases from 1 September 2002 to 20 March 2022: (a) Upper tropospheric carbon dioxide, 40°N–50°N zonal mean; (b) Mid-tropospheric methane, 40°N–50°N zonal mean. The plotted data are 15-day averages from the AIRS (CLIMCAPS-AQUA) daily Level 3 products and reveal both the annual cycles and the upward trends of these two key greenhouse gases. (Plots provided by Vivienne Payne and Paulo Penteado of the AIRS Science Team, with relabeling.)

4.4. Use of Aqua Data in Earth System Model Formulations and Evaluations

Aqua data have been widely used during the formulation and evaluation of Earth system models. In fact, the AIRS/AMSU, AMSR-E, CERES, and MODIS data are the most downloaded data sets in the Observations for Model Intercomparisons Project (Obs4MIP), which was created explicitly to facilitate the use of satellite data to evaluate the performance of Earth system models (Teixeira et al., 2014). Additionally, AIRS data have been used to constrain the water vapor feedback in models (Gordon et al., 2013) and to test model forecasts of cloud parameters (Garand et al., 2011), to evaluate Coupled Model Intercomparison Project Phase 5 (CMIP5) models (Tian et al., 2013), and to assess a climate model's cloud schemes (Stubenrauch et al., 2019) and a climate model's representation of atmospheric gravity waves (Holt et al., 2017); MODIS ocean color and SST data have been used in the modeling of ocean ecosystem dynamics (Mahadevan et al., 2012); and CERES data have been used

Figure 7. Sample Aqua Moderate Resolution Imaging Spectroradiometer imagery showing air quality issues: (a) Dust storm in the Middle East on 24 April 2022; (b) Fires and smoke in eastern Russia on 8 August 2021. (Images from NASA's Earth Observatory; the dust image is from https://earthobservatory.nasa.gov/images/149772/mediterranean-dust-storm, and the fire image is from https://earthobservatory.nasa.gov/images/148678/an-unusually-smoky-fire-season-in-sakha.)

to evaluate climate model parameterizations of clouds (Baran et al., 2016; Eidhammer et al., 2017) and deep convection (Wang & Zhang, 2016), to evaluate modeled top-of-the-atmosphere and surface radiative fluxes (Dolinar et al., 2015; Li et al., 2013; Loeb et al., 2022), and to provide insights on the surface radiative flux biases in CMIP5 global climate model (GCM) comparisons (Boeke & Taylor, 2016; Loew et al., 2016; Schneider & Reusch, 2016; X. Zhang, Liang, et al., 2016). These are just a few examples to illustrate the widespread use of Aqua data in model formulations and evaluations.

5. Practical Applications of Aqua Data

In addition to their scientific value, Aqua data have been widely used in practical applications. Notable examples include:

1. AIRS/AMSU data are routinely assimilated in near-real-time (generally within 2 hours of the observations) in operational weather prediction centers around the world. In fact, the AIRS instrument is recognized as one of the most important satellite instruments in the past 20 years for improving weather forecasts (Cardinali & Healy, 2012; Raju et al., 2015; Reale et al., 2018; WMO, 2012). It was the first advanced infrared sounder to be used operationally in numerical weather prediction (NWP), and experiences with AIRS have "played an important part in preparing the NWP community for rapidly exploiting the next generation of operational hyperspectral sounders," a sentiment expressed in a review article from the United Kingdom (UK) Met Office and the European Centre for Medium-Range Weather Forecasts (ECMWF) on NWP assimilation of satellite data (Eyre et al., 2022). Among the specific improvements, assimilation of AIRS data has been found to improve tropical cyclone forecasts at major NWP centers (Li et al., 2012; Liu & Zou, 2015) and to improve the representation of polar lows and a tropical-like cyclone in the Mediterranean Sea (Ganeshan et al., 2022).
2. MODIS-derived winds are also assimilated in operational forecast systems worldwide, with positive impact (e.g., Santek, 2010).
3. CERES data products from Aqua and Terra are available online at https://power.larc.nasa.gov within a week of the observations, through an effort of the Prediction of Worldwide renewable Energy Resource (POWER) project; and in the 4 years May 2018–May 2022, over 98 million data requests for these products were filled. Many of the requests have come from the agriculture and energy communities. The data support such agricultural efforts as crop modeling (Van Wart et al., 2015), assessment of regions for crop suitability, and estimation of potential evapotranspiration to help inform irrigation planning. Among the energy applications, the data are used to assess the performance of solar photovoltaic technologies (e.g., Armendariz-Lopez et al., 2016), to address issues regarding renewable energy and energy efficiency, and to monitor energy usage at the University of Michigan, Auburn University, NASA, 3M, Johnson Controls, and elsewhere.
4. MODIS data products regarding phytoplankton, cyanobacteria, and algae blooms have helped inform local populations of when these toxic water conditions exist or are imminent (e.g., Kahru et al., 2018). For one explicit example, the Aqua MODIS data are used along with numerical models in the California Harmful Algae Risk Mapping system in order to provide operational predictions of harmful conditions along the California coast, allowing better-informed management decisions by recreational managers, marine mammal rescue teams, and others (Anderson et al., 2016). For another example, Aqua MODIS data have identified and continue to monitor what since 2011 has become an annual development of a massive sargassum bloom stretching from the coast of western Africa westward to the Gulf of Mexico. Such monitoring can forewarn

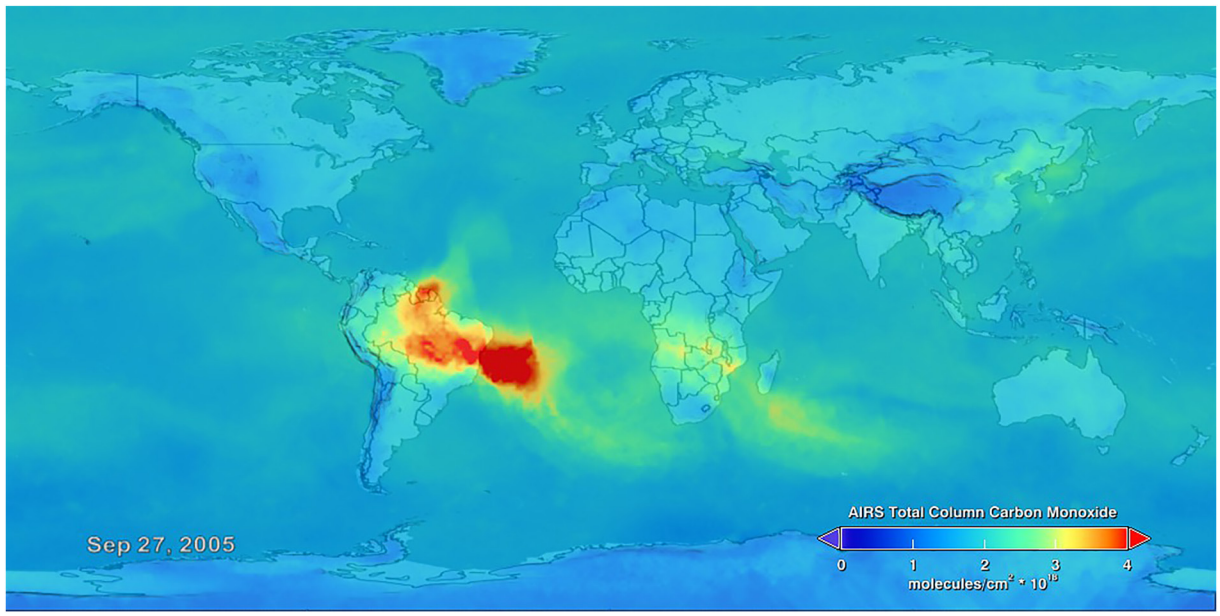

Figure 8. Global map of carbon monoxide on 27 September 2005, as derived from AIRS data, most prominently showing high levels of carbon monoxide in Brazil and off the Brazilian coast, due to fires burning in the Amazon and winds transporting the carbon monoxide eastward. (Image from the NASA Goddard Space Flight Center Scientific Visualization Studio, https://svs.gsfc.nasa.gov/3882, created by Lori Perkins, Tom Pagano, Edward Olsen, and Hai Nguyen.)

communities in its path of the approaching foul-smelling reddish-brown vegetation, often containing thick mats of seaweed (Wang et al., 2019).

5. AIRS/AMSU sulfur dioxide data, often highlighting volcanic emissions, are used operationally by NOAA to notify the Volcanic Ash Advisory Center when high sulfur dioxide concentrations exist, for the purpose of assisting pilots in avoiding aviation hazards; and MODIS data on volcanic emissions are used by the Federal Aviation Administration for the same purpose. In the specific case of the eruption of Iceland's Eyjafjallajokull volcano in April and May 2010, both MODIS and AIRS imagery were used in determinations of flight cancellations and rerouting of flights to, from, and within Europe at that time (Prata & Prata, 2012; Walker et al., 2012). AIRS data are also used by the European Space Agency's Support to Aviation Control Service for near-real-time monitoring of volcanic plumes (Brenot et al., 2014).
6. AIRS near-surface humidity data are used by the County of Los Angeles, California, in a semi-operational prediction system for influenza outbreaks. More broadly, the AIRS data have been used to determine geographically variable threshold values of humidity that signal the likely onset of flu breakouts throughout the contiguous United States (U.S.) (Serman et al., 2022).
7. The County of Los Angeles uses MODIS land surface temperatures in efforts to develop climate adaptation and mitigation strategies (Hulley et al., 2019).
8. MODIS data have been used by the U.S. Department of Agriculture, other operational agencies, and the International Group on Earth Observations Global Agricultural Monitoring (GEOGLAM) project to monitor the condition of crops during the growing season. Of particular importance, this satellite-based monitoring, incorporating MODIS data, can provide early identification of poor crop production in food-insecure countries and lead to timely mobilization of food aid (Becker-Reshef et al., 2020). The MODIS data have also been shown to improve the timeliness of forecasts of winter wheat production in the U.S., Ukraine, and China (Franch et al., 2015).
9. MODIS images provide clear depictions of forest fires, dust storms, and oil spills, allowing communities potentially affected by these events to readily monitor them (e.g., Figure 7). The fire imagery in particular can assist forest services in decisions regarding the deployment of firefighters.
10. MODIS data are also used for sea ice monitoring by the Canadian Ice Service, the NOAA CoastWatch program, and the U.S. Coast Guard.

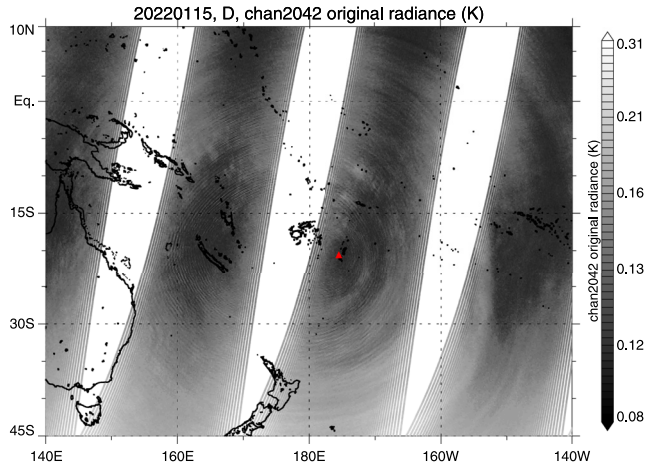

Figure 9. Atmospheric gravity waves propagating from the 15 January 2022, Hunga Tonga-Hunga Ha'apai volcanic eruption in the south Pacific, as revealed in the Atmospheric Infrared Sounder (AIRS) channel 2042 radiances. (Image from Tao Wang of the AIRS Science Team.)

11. While AMSR-E was still operating, AMSR-E data were used in hurricane monitoring efforts at the U.S. National Hurricane Center, the U.S. Navy and Air Force Joint Typhoon Warning Center, and the Japan Meteorological Agency.

6. Discussion

With Aqua data incorporated in over 20,000 scientific publications, this paper by necessity only presents a small fraction of results obtained from Aqua. Additional exciting areas of research with Aqua data include: (a) the use of AIRS data to study atmospheric gravity waves (e.g., Kalisch & Chun, 2021; Yao et al., 2022), including the first global maps of convectively-generated concentric gravity waves (Gong et al., 2015) and images of the waves generated from the January 2022 Hunga Tonga-Hunga Ha'apai eruption (Figure 9); (b) the use of AIRS data to reveal significant increases in ammonia over major agricultural regions, likely due to increased fertilizer usage and animal husbandry (Warner et al., 2017); (c) the joint use of AIRS CO_2 data and MODIS gross primary productivity data to examine the drawdown of atmospheric CO_2 into the boreal forests (Pagano et al., 2014); (d) the use of MODIS data to monitor and analyze the Great Calcite Belt in the Southern Ocean (Balch et al., 2016; Smith et al., 2017); and (e) the use of CERES data to examine northward Atlantic Ocean heat transport (Trenberth & Fasullo, 2017).

For studies of climate and Earth system changes, the length of the record is enormously important, and much work has gone into extending earlier records with Aqua data and extending Aqua data with data records that could continue beyond Aqua. Examples of the former include: Franz et al. (2016) and Sathyendranath et al. (2019) using MODIS data to extend ocean chlorophyll-a records from the Sea-viewing Wide-Field-of-view Sensor (SeaWiFS); Oziel et al. (2022) using data from the Coastal Zone Color Scanner to further extend the SeaWiFS and Aqua MODIS chlorophyll-a records back to 1979; Dorigo et al. (2012) using AMSR-E data to extend soil moisture records from the Special Sensor Microwave Imager; and Allan et al. (2014) using CERES data to extend Earth radiation budget records from the Earth Radiation Budget Satellite. Examples of extending Aqua data with records that either have continued or could continue beyond the relevant Aqua measurements include the extension of AMSR-E records with AMSR2 data (e.g., Du et al., 2017 for soil moisture and other land parameters; Meier & Ivanoff, 2017 for sea ice concentrations), the extension of Aqua CERES records with records from the CERES on Suomi NPP and NOAA-20 (e.g., Loeb & Doelling, 2020), the extension of AIRS records with records from the Cross-track Infrared Sounder (CrIS) (e.g., Aumann et al., 2016; Motteler & Strow, 2019), and the extension of MODIS records with records from the Visible Infrared Imaging Radiometer Suite (e.g., Levy et al., 2015 and Sayer et al., 2017, 2019 for aerosols; Franz et al., 2016 for chlorophyll-a; Hall et al., 2019 for snow cover extent; and Skakun et al., 2018 for vegetation). Like all satellite missions, the Aqua mission will end at some point. However, it is encouraging to know that many of the data records meticulously created with Aqua data will be extended into the future by records from other, later missions.

Data Availability Statement

The Aqua data are archived and publicly available at the following data centers: The Goddard Earth Sciences (GES) Data and Information Services Center (DISC) for AIRS, AMSU, and HSB data (disc.gsfc.nasa.gov/AIRS); the National Snow and Ice Data Center (NSIDC) for AMSR-E data (nsidc.org/data/amsre) and for MODIS snow and ice data (nsidc.org/data/modis); the Langley Research Center (LaRC) Distributed Active Archive Center (DAAC) for CERES data (eosweb.larc.nasa.gov); the Land Processes DAAC (LPDAAC) for MODIS land data (lpdaac.usgs.gov); the Level 1 and Atmosphere Archive and Distribution System (LAADS) DAAC for MODIS atmosphere data (ladsweb.nascom.nasa.gov); the Ocean Biology Processing Group (OBPG) data repository for MODIS ocean color data (oceancolor.gsfc.nasa.gov); and the Physical Oceanography DAAC (PODAAC) for MODIS sea surface temperature data (podaac.jpl.nasa.gov/datasetlist?-searchAQUA). The Aqua MODIS data plotted in Figure 5 are available at https://doi.org/10.5067/MODIS/

MYD08_M3.061 and the Terra MODIS data plotted in Figure 5 are available at https://doi.org/10.5067/MODIS/MOD08_M3.061, both with reference Platnick, King, and Hubanks (2017). The AIRS data plotted in Figure 6 are available at https://doi.org/10.5067/47IB56XWPHB3, with the carbon dioxide data in the CLIMCAPS file co2_vmr_uppertrop and the methane data in the CLIMCAPS file ch4_mmr_midtrop (Barnet, 2019).

Acknowledgments
Funding for this work came through the NASA Headquarters Earth Science Division's funding for the Aqua Earth-observing mission and is much appreciated. Many thanks also go to Joao Teixeira and Eric Fetzer from the AIRS Science Team and the anonymous reviewers for reading through and offering valuable comments on the manuscript, to Lazaros Oreopoulos from Aqua science leadership for discussions on the Aqua mission, to Norman Loeb from the CERES Science Team for CERES references, to Paul Stackhouse from Langley Research Center for POWER project statistics, to Bill Guit and Jamie Pawloski from the ESMO Project for operational dates provided in Table 1, to the NASA EOS Data and Information System (EOSDIS) for its Worldview application making Figure 4 possible, and to the following people for help with the figures: Bill Guit from the ESMO Project; Carl Martin from Northrop Grumman; Joao Teixeira, Eric Fetzer, Vivienne Payne, Paulo Penteado, and Tao Wang from the AIRS Science Team; Michael King from the MODIS Science Team; and Nandana Amarasinghe and Nick DiGirolamo from Science Systems and Applications, Inc.

References

Adame, J. A., Lope, L., Hidalgo, P. J., Sorribas, M., Gutiérrez-Álvarez, I., Del Águila, A., et al. (2018). Study of the exceptional meteorological conditions, trace gases and particulate matter measured during the 2017 forest fire in Doñana Natural Park, Spain. *Science of the Total Environment*, *645*, 710–720. https://doi.org/10.1016/j.scitotenv.2018.07.181

Allan, R. P., Liu, C., Loeb, N. G., Palmer, M. D., Roberts, M., Smith, D., & Vidale, P.-L. (2014). Changes in global net radiative imbalance 1985–2012. *Geophysical Research Letters*, *41*(15), 5588–5597. https://doi.org/10.1002/2014GL060962

Anderson, C. R., Kudela, R. M., Kahru, M., Chao, Y., Rosenfeld, L. K., Bahr, F. L., et al. (2016). Initial skill assessment of the California harmful algae risk mapping (CHARM) system. *Harmful Algae*, *59*, 1–18. https://doi.org/10.1016/j.hal.2016.08.006

Armendariz-Lopez, J. F., Luna-Leon, A., Gonzalez-Trevizo, M. E., Arena-Granados, A. P., & Bojorquez-Morales, G. (2016). Life cycle cost of photovoltaic technologies in commercial buildings in Baja California, Mexico. *Renewable Energy*, *87*(1), 564–571. https://doi.org/10.1016/j.renene.2015.10.051

Aumann, H. H., Chahine, M. T., Gautier, C., Goldberg, M. D., Kalnay, E., McMillin, L. M., et al. (2003). AIRS/AMSU/HSB on the Aqua mission: Design, science objectives, data products, and processing systems. *IEEE Transactions on Geoscience and Remote Sensing*, *41*(2), 253–264. https://doi.org/10.1109/tgrs.2002.808356

Aumann, H. H., Elliott, D., & Manning, E. (2016). Comparison of the AIRS, IASI, and CrIS 900 cm-1 channel for Dome Concordia. In *Proceedings of the Society of Photo-Optical Instrumentation Engineers Earth Observing Systems* (Vol. XXI). https://doi.org/10.1117/12.2235945

Balch, W. M., Bates, N. R., Lam, P. J., Twining, B. S., Rosengard, S. Z., Bowler, B. C., et al. (2016). Factors regulating the Great Calcite Belt in the Southern Ocean and its biogeochemical significance. *Global Biogeochemical Cycles*, *30*(8), 1124–1144. https://doi.org/10.1002/2016gb005414

Baran, A. J., Hill, P., Walters, D., Hardiman, S. C., Furtado, K., Field, P. R., & Manners, J. (2016). The impact of two coupled cirrus microphysics-radiation parameterizations on the temperature and specific humidity biases in the tropical tropopause layer in a climate model. *Journal of Climate*, *29*(14), 5299–5316. https://doi.org/10.1175/JCLI-D-15-0821.1

Barnes, W. L., Pagano, T. S., & Salomonson, V. V. (1998). Prelaunch characteristics of the moderate resolution imaging spectroradiometer (MODIS) on EOS-AM1. *IEEE Transactions on Geoscience and Remote Sensing*, *36*(4), 1088–1100. https://doi.org/10.1109/36.700993

Barnet, C. (2019). *Sounder SIPS: Aqua AIRS IR-only Level 3 CLIMCAPS: Specific quality control gridded daily V2*. Goddard Earth Sciences Data and Information Services Center (GES DISC). https://doi.org/10.5067/47IB56XWPHB3

Becker-Reshef, I., Justice, C., Barker, B., Humber, M., Rembold, F., Bonifacio, R., et al. (2020). Strengthening agricultural decisions in countries at risk of food insecurity: The GEOGLAM crop monitor for early warning. *Remote Sensing of Environment*, *237*, 111553. https://doi.org/10.1016/j.rse.2019.111553

Bhagat, V. S. (2015). Space-borne passive microwave remote sensing of soil moisture: A review. *Recent Progress in Space Technology*, *4*(2), 119–150. https://doi.org/10.2174/2210687104021505131231 46

Boeke, R. C., & Taylor, P. C. (2016). Evaluation of the Arctic surface radiation budget in CMIP5 models. *Journal of Geophysical Research: Atmospheres*, *121*(14), 8525–8548. https://doi.org/10.1002/2016JD025099

Boisvert, L., Vihma, T., & Shie, C.-L. (2020). Evaporation from the Southern Ocean estimated on the basis of AIRS satellite data. *Journal of Geophysical Research: Atmospheres*, *125*(1), e2019JD030845. https://doi.org/10.1029/2019JD030845

Boisvert, L. N., Markus, T., & Vihma, T. (2013). Moisture flux changes and trends for the entire Arctic in 2003-2011 derived from EOS Aqua data. *Journal of Geophysical Research: Oceans*, *118*(10), 5829–5843. https://doi.org/10.1002/jgrc.20414

Brenot, H., Theys, N., Clarisse, L., van Geffen, J., van Gent, J., Van Roozendael, M., et al. (2014). Support to Aviation Control Service (SACS): An online service for near-real-time satellite monitoring of volcanic plumes. *Natural Hazards and Earth System Sciences*, *14*(5), 1099–1123. https://doi.org/10.5194/nhess-14-1099-2014

Brient, F., & Schneider, T. (2016). Constraints on climate sensitivity from space-based measurements of low-cloud reflection. *Journal of Climate*, *29*(16), 5821–5835. https://doi.org/10.1175/JCLI-D-15-0897.1

Buchholz, R. R., Worden, H. M., Park, M., Francis, G., Deeter, M. N., Edwards, D. P., et al. (2021). Air pollution trends measured from Terra: CO and AOD over industrial, fire-prone, and background regions. *Remote Sensing of Environment*, *256*, 112275. https://doi.org/10.1016/j.rse.2020.112275

Cardinali, C., & Healy, S. (2012). Forecast sensitivity to observation error variance. *ECMWF Newsletter*, *133*, 30–33.

Chahine, M., Barnet, C., Olsen, E. T., Chen, L., & Maddy, E. (2005). On the determination of atmospheric minor gases by the method of vanishing partial derivatives with application to CO_2. *Geophysical Research Letters*, *32*(22), L22803. https://doi.org/10.1029/2005GL024165

Chahine, M. T., Chen, L., Dimotakis, P., Jiang, X., Li, Q., Olsen, E. T., et al. (2008). Satellite remote sounding of mid-tropospheric CO_2. *Geophysical Research Letters*, *35*(17), L17807. https://doi.org/10.1029/2008GL035022

Dolinar, E. K., Dong, X., Xi, B., Jiang, J. H., & Su, H. (2015). Evaluation of CMIP5 simulated clouds and TOA radiation budgets using NASA satellite observations. *Climate Dynamics*, *44*(7–8), 2229–2247. https://doi.org/10.1007/s00382-014-2158-9

Dorigo, W., de Jeu, R., Chung, D., Parinussa, R., Liu, Y., Wagner, W., & Fernandez-Prieto, D. (2012). Evaluating global trends (1988–2010) in harmonized multi-satellite surface soil moisture. *Geophysical Research Letters*, *39*(18), L18405. https://doi.org/10.1029/2012GL052988

Du, J., Kimball, J. S., Jones, L. A., Kim, Y., Glassy, J., & Watts, J. D. (2017). A global satellite environmental data record derived from AMSR-E and AMSR2 microwave Earth observations. *Earth System Science Data*, *9*(2), 791–808. https://doi.org/10.5194/essd-9-791-2017

Eidhammer, T., Morrison, H., Mitchell, D., Gettelman, A., & Erfani, E. (2017). Improvements in global climate model microphysics using a consistent representation of ice particle properties. *Journal of Climate*, *30*(2), 609–629. https://doi.org/10.1175/JCLI-D-16-0050.1

Eyre, J. R., Bell, W., Cotton, J., English, S. J., Forsythe, M., Healy, S. B., & Pavelin, E. G. (2022). Assimilation of satellite data in numerical weather prediction. Part II: Recent years. *Quarterly Journal of the Royal Meteorological Society*, *148*(743), 521–556. https://doi.org/10.1002/qj.4228

Farahmand, A., AghaKouchak, A., & Teixeira, J. (2015). A vantage from space can detect earlier drought onset: An approach using relative humidity. *Scientific Reports*, *5*(1), 8553. https://doi.org/10.1038/srep08553

Fayne, J. V., Bolten, J. D., Doyle, C. S., Fuhrmann, S., Rice, M. T., Houser, P. R., & Lakshmi, V. (2017). Flood mapping in the lower Mekong River Basin using daily MODIS observations. *International Journal of Remote Sensing*, *38*(6), 1737–1757. https://doi.org/10.1080/01431161.2017.1285503

Field, R. D., van der Werf, G. R., Fanin, T., Fetzer, E. J., Fuller, R., Jethva, H., et al. (2016). Indonesian fire activity and smoke pollution in 2015 show persistent nonlinear sensitivity to El Nino-induced drought. *Proceedings of the National Academy of Sciences of the United States of America*, *113*(33), 9204–9209. https://doi.org/10.1073/pnas.1524888113

Franch, B., Vermote, E. F., Becker-Reshef, I., Claverie, M., Huang, J., Zhang, J., et al. (2015). Improving the timeliness of winter wheat production forecast in the United States of America, Ukraine and China using MODIS data and NCAR Growing Degree Day information. *Remote Sensing of Environment*, *161*, 131–148. https://doi.org/10.1016/j.rse.2015.02.014

Franz, B. A., Behrenfeld, M. J., Siegel, D. A., & Signorini, S. R. (2016). Global ocean phytoplankton [in State of the Climate in 2015]. *Bulletin of the American Meteorological Society*, *97*, S87–S89.

Ganeshan, M., Reale, O., McGrath-Spangler, E., & Boukachaba, N. (2022). Impact of assimilating adaptively thinned AIRS cloud-cleared radiances on the analysis of polar lows and Mediterranean Sea tropical-like cyclone in a global modeling and data assimilation framework. *Weather and Forecasting*, *37*(7), 1117–1134. https://doi.org/10.1175/WAF-D-21-0068.1

Garand, L., Pancrati, O., & Heilliette, S. (2011). Validation of forecast cloud parameters from multispectral AIRS radiances. *Atmosphere-Ocean*, *49*(2), 121–137. https://doi.org/10.1080/07055900.2011.567379

Gong, J., Yue, J., & Wu, D. L. (2015). Global survey of concentric gravity waves in AIRS images and ECMWF analysis. *Journal of Geophysical Research: Atmospheres*, *120*(6), 2210–2228. https://doi.org/10.1002/2014JD022527

Gordon, N. D., Jonko, A. K., Forster, P. M., & Shell, K. M. (2013). An observationally based constraint on the water-vapor feedback. *Journal of Geophysical Research: Atmospheres*, *118*(22), 12435–12443. https://doi.org/10.1002/2013JD020184

Hall, D. K., Riggs, G. A., DiGirolamo, N. E., & Roman, M. O. (2019). Evaluation of MODIS and VIIRS cloud-gap-filled snow-cover products for production of an Earth science data record. *Hydrology and Earth System Sciences*, *23*(12), 5227–5241. https://doi.org/10.5194/hess-23-5227-2019

Hari, M., Sahu, R. K., Sunder, M. S., & Tyagi, B. (2022). Then and now: COVID-19 pandemic lockdown misfire atmospheric methane over India. *Aerosol and Air Quality Research*, *22*(4), 210354. https://doi.org/10.4209/aaqr.210354

Holt, L. A., Alexander, M. J., Coy, L., Liu, C., Molod, A., Putman, W., & Pawson, S. (2017). An evaluation of gravity waves and gravity wave sources in the Southern Hemisphere in a 7 km global climate simulation. *Quarterly Journal of the Royal Meteorological Society*, *143*(707), 2481–2495. https://doi.org/10.1002/qj.3101

Hsu, N. C., Li, C., Krotkov, N. A., Liang, Q., Yang, K., & Tsay, S.-C. (2012). Rapid transpacific transport in autumn observed by the A-train satellites. *Journal of Geophysical Research*, *117*(D6), D06312. https://doi.org/10.1029/2011JD016626

Huang, M., Carmichael, G. R., Pierce, R. B., Jo, D. S., Park, R. J., Flemming, J., et al. (2017). Impact of intercontinental pollution transport on North American ozone air pollution: An HTAP phase 2 multi-model study. *Atmospheric Chemistry and Physics*, *17*(9), 5721–5750. https://doi.org/10.5194/acp-17-5721-2017

Huang, X., Chen, X., Potter, G. L., Oreopoulos, L., Cole, J. N. S., Lee, D., & Loeb, N. G. (2014). A global climatology of outgoing longwave spectral cloud radiative effect and associated effective cloud properties. *Journal of Climate*, *27*(19), 7475–7492. https://doi.org/10.1175/jcli-d-13-00663.1

Hulley, G., Shivers, S., Wetherley, E., & Cudd, R. (2019). New ECOSTRESS and MODIS land surface temperature data reveal fine-scale heat vulnerability in cities: A case study for Los Angeles county, California. *Remote Sensing*, *11*(18), 2136. https://doi.org/10.3390/rs11182136

Irion, F. W., Kahn, B. H., Schreier, M. M., Fetzer, E. J., Fishbein, E., Fu, D., et al. (2018). Single-footprint retrievals of temperature, water vapor and cloud properties from AIRS. *Atmospheric Measurement Techniques*, *11*(2), 971–995. https://doi.org/10.5194/amt-11-971-2018

Jackson, T. J., Bindlish, R., & Cosh, M. (2009). Validation of AMSR-E soil moisture products using in situ observations. *Journal of the Remote Sensing Society of Japan*, *29*(1), 263–270.

Joseph, R., Smith, T. M., Sapiano, M. R. P., & Ferraro, R. R. (2009). A new high-resolution satellite-derived precipitation dataset for climate studies. *Journal of Hydrometeorology*, *10*(4), 935–952. https://doi.org/10.1175/2009jhm1096.1

Kahn, B. H., Irion, F. W., Dang, V. T., Manning, E. M., Nasiri, S. L., Naud, C. M., et al. (2014). The atmospheric infrared sounder version 6 cloud products. *Atmospheric Chemistry and Physics*, *14*(1), 399–426. https://doi.org/10.5194/acp-14-399-2014

Kahru, M., Elmgren, R., di Lorenzo, E., & Savchuk, O. P. (2018). Unexplained interannual oscillations of cyanobacterial blooms in the Baltic Sea. *Scientific Reports*, *8*(1), 6365. https://doi.org/10.1038/s41598-018-24829-7

Kalisch, S., & Chun, H.-Y. (2021). AIRS satellite observations of gravity waves during the 2009 sudden stratospheric warming event. *Journal of Geophysical Research: Atmospheres*, *126*(4), e2020JD034073. https://doi.org/10.1029/2020JD034073

Kawanishi, T., Sezai, T., Ito, Y., Imaoka, K., Takeshima, T., Ishido, Y., et al. (2003). The advanced microwave scanning radiometer for the Earth observing system (AMSR-E), NASDA's contribution to the EOS for global energy and water cycle studies. *IEEE Transactions on Geoscience and Remote Sensing*, *41*(2), 184–194. https://doi.org/10.1109/tgrs.2002.808331

Kilpatrick, K. A., Podesta, G., Walsh, S., Williams, E., Halliwell, V., Szczodrak, M., et al. (2015). A decade of sea surface temperature from MODIS. *Remote Sensing of Environment*, *165*, 27–41. https://doi.org/10.1016/j.rse.2015.04.023

Kim, B., & Sarkar, S. (2017). Impact of wildfires on some greenhouse gases over continental USA: A study based on satellite data. *Remote Sensing of Environment*, *188*, 118–126. https://doi.org/10.1016/j.rse.2016.10.047

King, M. D., Platnick, S., Menzel, W. P., Ackerman, S. A., & Hubanks, P. A. (2013). Spatial and temporal distribution of clouds observed by MODIS onboard the Terra and Aqua satellites. *IEEE Transactions on Geoscience and Remote Sensing*, *51*(7), 3826–3852. https://doi.org/10.1109/tgrs.2012.2227333

Lambrigtsen, B. H. (2003). Calibration of the AIRS microwave instruments. *IEEE Transactions on Geoscience and Remote Sensing*, *41*(2), 369–378. https://doi.org/10.1109/tgrs.2002.808247

Lambrigtsen, B. H., & Calheiros, R. V. (2003). The humidity sounder for Brazil – An international partnership. *IEEE Transactions on Geoscience and Remote Sensing*, *41*(2), 352–361. https://doi.org/10.1109/tgrs.2002.808304

Levy, R. C., Munchak, L. A., Mattoo, S., Patadia, F., Remer, L. A., & Holz, R. E. (2015). Towards a long-term global aerosol optical depth record: Applying a consistent aerosol retrieval algorithm to MODIS and VIIRS-observed reflectance. *Atmospheric Measurement Techniques*, *8*(10), 4083–4110. https://doi.org/10.5194/amt-8-4083-2015

Li, J., Li, J., Zheng, J., & Schmit, T. (2012). Improving tropical cyclone forecasts with water vapor and temperature information from satellites. *Joint Center for Satellite Data Assimilation (JCSDA) Quarterly*, *38*, 1–2.

Li, J.-L. F., Waliser, D. E., Stephens, G., Lee, S., L'Ecuyer, T., Kato, S., et al. (2013). Characterizing and understanding radiation budget biases in CMIP3/CMIP5 GCMs, contemporary GCM, and reanalysis. *Journal of Geophysical Research: Atmospheres*, *118*(15), 8166–8184. https://doi.org/10.1002/jgrd.50378

Lin, M., Fiore, A. M., Horowitz, L. W., Cooper, O. R., Naik, V., Holloway, J., et al. (2012). Transport of Asian ozone pollution into surface air over the western United States in spring. *Journal of Geophysical Research*, *117*(D21), D00V07. https://doi.org/10.1029/2011jd016961

Liu, Y., & Zou, X. L. (2015). Impact of 4DVAR assimilation of AIRS total column ozone observations on the simulation of Hurricane Earl. *Journal of Meteorological Research*, *29*(2), 257–271. https://doi.org/10.1007/s13351-015-4058-2

Loeb, N. G., & Doelling, D. R. (2020). CERES energy balanced and filled (EBAF) from afternoon-only satellite orbits. *Remote Sensing*, *12*(8), 1280. https://doi.org/10.3390/rs12081280

Loeb, N. G., Lyman, J. M., Johnson, G. C., Allan, R. P., Doelling, D. R., Wong, T., et al. (2012). Observed changes in top-of-the-atmosphere radiation and upper-ocean heating consistent within uncertainty. *Nature Geoscience*, *5*(2), 110–113. https://doi.org/10.1038/ngeo1375

Loeb, N. G., Mayer, M., Kato, S., Fasullo, J. T., Zuo, H., Senan, R., et al. (2022). Evaluating twenty-year trends in Earth's energy flows from observations and reanalyses. *Journal of Geophysical Research: Atmospheres*, *127*(12), e2022JD036686. https://doi.org/10.1029/2022JD036686

Loew, A., Andersson, A., Trentmann, J., & Schröder, M. (2016). Assessing surface solar radiation fluxes in the CMIP ensembles. *Journal of Climate*, *29*(20), 7231–7246. https://doi.org/10.1175/JCLI-D-14-00503.1

Mahadevan, A., D'Asaro, E., Lee, C., & Perry, M.-J. (2012). Eddy-driven stratification initiates North Atlantic spring phytoplankton blooms. *Science*, *337*(6090), 54–58. https://doi.org/10.1126/science.1218740

Meier, W. N., & Ivanoff, A. (2017). Intercalibration of AMSR2 NASA Team 2 algorithm sea ice concentrations with AMSR-E slow rotation data. *IEEE Journal of Selected Topics in Applied Earth Observations and Remote Sensing*, *10*(9), 3923–3933. https://doi.org/10.1109/JSTARS.2017.2719624

Miller, D. J., Sun, K., Zondlo, M. A., Kanter, D., Dubovik, O., Welton, E. J., et al. (2011). Assessing boreal forest fire smoke aerosol impacts on U.S. air quality: A case study using multiple data sets. *Journal of Geophysical Research*, *116*(D22), D22209. https://doi.org/10.1029/2011JD016170

Mo, T. (1996). Prelaunch calibration of the advanced microwave sounding unit-A for NOAA-K. *IEEE Transactions on Microwave Theory and Techniques*, *44*(8), 1460–1469. https://doi.org/10.1109/22.536029

Motteler, H., & Strow, L. L. (2019). AIRS deconvolution and the translation of AIRS-to-CrIS radiances with applications for the IR climate record. *IEEE Transactions on Geoscience and Remote Sensing*, *57*(3), 1793–1803. https://doi.org/10.1109/TGRS.2018.2869170

Mu, Q. Z., Zhao, M. S., & Running, S. W. (2011). Improvements to a MODIS global terrestrial evapotranspiration algorithm. *Remote Sensing of Environment*, *115*(8), 1781–1800. https://doi.org/10.1016/j.rse.2011.02.019

Naud, C. M., & Kahn, B. H. (2015). Thermodynamic phase and ice cloud properties in northern hemisphere winter extratropical cyclones observed by Aqua AIRS. *Journal of Applied Meteorology and Climatology*, *54*(11), 2283–2303. https://doi.org/10.1175/JAMC-D-15-0045.1

Nielsen-Englyst, P., Hoyer, J. L., Pedersen, L. T., Gentemann, C. L., Alerskans, E., Block, T., & Donlon, C. (2018). Optimal estimation of sea surface temperature from AMSR-E. *Remote Sensing*, *10*(2), 229. https://doi.org/10.3390/rs10020229

Nishida, K., Nemani, R. R., Running, S. W., & Glassy, J. M. (2003). An operational remote sensing algorithm of land surface evaporation. *Journal of Geophysical Research*, *108*(D9), 4270. https://doi.org/10.1029/2002jd002062

Oreopoulos, L., Cho, N., Lee, D., & Kato, S. (2016). Radiative effects of global MODIS cloud regimes. *Journal of Geophysical Research: Atmospheres*, *121*(5), 2299–2317. https://doi.org/10.1002/015JD024502

Oziel, L., Massicotte, P., Babin, M., & Devred, E. (2022). Decadal changes in Arctic Ocean chlorophyll a: Bridging ocean color observations from the 1980s to present time. *Remote Sensing of Environment*, *275*, 113020. https://doi.org/10.1016/j.rse.2022.113020

Pagano, T. S., Johnson, D. L., McGuire, J. P., Schwochert, M. A., & Ting, D. Z. (2022). Technology maturation efforts for the next generation of grating spectrometer hyperspectral infrared sounders. *IEEE Journal of Selected Topics in Applied Earth Observations and Remote Sensing*, *15*, 2929–2943. https://doi.org/10.1109/jstars.2022.3165168

Pagano, T. S., Olsen, E. T., Nguyen, H., Ruzmaikin, A., Jiang, X., & Perkins, L. (2014). Global variability of midtropospheric carbon dioxide as measured by the atmospheric infrared sounder. *Journal of Applied Remote Sensing*, *8*(01), 1. https://doi.org/10.1117/1.JRS.8.084984

Petri, C. A., & Galvao, L. S. (2019). Sensitivity of seven MODIS vegetation indices to BRDF effects during the Amazonian dry season. *Remote Sensing*, *11*(14), 1650. https://doi.org/10.3390/rs11141650

Pistone, K., Eisenman, I., & Ramanathan, V. (2019). Radiative heating of an ice-free Arctic Ocean. *Geophysical Research Letters*, *46*(13), 7474–7480. https://doi.org/10.1029/2019GL082914

Platnick, S., King, M., & Hubanks, P. (2017). *MODIS atmosphere L3 monthly product. NASA MODIS adaptive processing system*. Goddard Space Flight Center. https://doi.org/10.5067/MODIS/MYD08_M3.061 for the Aqua data and https://doi.org/10.5067/MODIS/MOD08_M3.061 for the Terra data

Platnick, S., Meyer, K. G., King, M. D., Wind, G., Amarasinghe, N., Marchant, B., et al. (2017). The MODIS cloud optical and microphysical products: Collection 6 updates and examples from Terra and Aqua. *IEEE Transactions on Geoscience and Remote Sensing*, *55*(1), 502–525. https://doi.org/10.1109/tgrs.2016.2610522

Prata, A. J., & Prata, A. T. (2012). Eyjafjallajökull volcanic ash concentrations determined using spin enhanced visible and infrared imager measurements. *Journal of Geophysical Research*, *117*(D20), D00U23. https://doi.org/10.1029/2011JD016800

Raju, A., Parekh, A., Kumar, P., & Gnanaseelan, C. (2015). Evaluation of the impact of AIRS profiles on prediction of Indian summer monsoon using WRF variational data assimilation system. *Journal of Geophysical Research: Atmospheres*, *120*(16), 8112–8131. https://doi.org/10.1002/2014JD023024

Reale, O., McGrath-Spangler, E. L., McCarty, W., Holdaway, D., & Gelaro, R. (2018). Impact of adaptively thinned AIRS cloud-cleared radiances on tropical cyclone representation in a global data assimilation and forecast system. *Weather and Forecasting*, *33*(4), 909–931. https://doi.org/10.1175/WAF-D-17-0175.1

Santek, D. (2010). The impact of satellite-derived polar winds on lower-latitude forecasts. *Monthly Weather Review*, *138*(1), 123–139. https://doi.org/10.1175/2009mwr2862.1

Sathyendranath, S., Brewin, R. J. W., Brockmann, C., Brotas, V., Calton, B., Chuprin, A., et al. (2019). An ocean-colour time series for use in climate studies: The experience of the ocean-colour climate change initiative (OC-CCI). *Sensors*, *19*, 4285. https://doi.org/10.3390/s19194285

Sayer, A. M., Hsu, N. C., Bettenhausen, C., Holz, R. E., Lee, L., Quinn, G., & Veglio, P. (2017). Cross calibration of S-NPP VIIRS moderate-resolution reflective solar bands against MODIS Aqua over dark water scenes. *Atmospheric Measurement Techniques*, *10*(4), 1425–1444. https://doi.org/10.5194/amt-10-1425-2017

Sayer, A. M., Hsu, N. C., Lee, J., Kim, W. V., & Dutcher, S. T. (2019). Validation, stability, and consistency of MODIS collection 6.1 and VIIRS version 1 deep blue aerosol data over land. *Journal of Geophysical Research*, *124*(8), 4658–4688. https://doi.org/10.1029/2018jd029598

Schneider, D. P., & Reusch, D. B. (2016). Antarctic and Southern Ocean surface temperatures in CMIP5 models in the context of the surface energy budget. *Journal of Climate*, *29*(5), 1689–1716. https://doi.org/10.1175/JCLI-D-15-0429.1

Serman, E., Thrastarson, H. T., Franklin, M., & Teixeira, J. (2022). Spatial variation in humidity and the onset of seasonal influenza across the contiguous United States. *GeoHealth*, *6*(2), e2021GH000469. https://doi.org/10.1029/2021GH000469

Skakun, S., Justice, C. O., Vermote, E., & Roger, J. C. (2018). Transitioning from MODIS to VIIRS: An analysis of inter-consistency of NDVI data sets for agricultural monitoring. *International Journal of Remote Sensing*, *39*(4), 971–992. https://doi.org/10.1080/01431161.2017.1395970

Smith, H. E. K., Poulton, A. J., Garley, R., Hopkins, J., Lubelczyk, L. C., Drapeau, D. T., et al. (2017). The influence of environmental variability on the biogeography of coccolithophores and diatoms in the Great Calcite Belt. *Biogeosciences*, *14*(21), 4905–4925. https://doi.org/10.5194/bg-14-4905-2017

Strow, L. L., & Hannon, S. E. (2008). A 4-year zonal climatology of lower tropospheric CO_2 derived from ocean-only atmospheric infrared sounder observations. *Journal of Geophysical Research*, *113*(D18), D18302. https://doi.org/10.1029/2007JD009713

Stubenrauch, C. J., Bonazzola, M., Protopapadaki, S. E., & Musat, I. (2019). New cloud system metrics to assess bulk ice cloud schemes in a GCM. *Journal of Advances in Modeling Earth Systems*, *11*(10), 3212–3234. https://doi.org/10.1029/2019MS001642

Susskind, J., Schmidt, G. A., Lee, J. N., & Iredell, L. (2019). Recent global warming as confirmed by AIRS. *Environmental Research Letters*, *14*(4), 044030. https://doi.org/10.1088/1748-9326/aafd4e

Teixeira, J., Waliser, D., Ferraro, R., Gleckler, P., Lee, T., & Potter, G. (2014). Satellite observations for CMIP5: The genesis of Obs4MIPs. *Bulletin of the American Meteorological Society*, *95*(9), 1329–1334. https://doi.org/10.1175/bams-d-12-00204.1

Temimi, M., Lacava, T., Lakhankar, T., Tramutoli, V., Ghedira, H., Ata, R., & Khanbilvardi, R. (2011). A multitemporal analysis of AMSR-E data for flood and discharge monitoring during the 2008 flood in Iowa. *Hydrological Processes*, *25*(16), 2623–2634. https://doi.org/10.1002/hyp.8020

Tian, B., Fetzer, E. J., Kahn, B. H., Teixeira, J., Manning, E., & Hearty, T. (2013). Evaluating CMIP5 models using AIRS tropospheric air temperature and specific humidity climatology. *Journal of Geophysical Research: Atmospheres*, *118*(1), 114–134. https://doi.org/10.1029/2012JD018607

Trenberth, K. E., & Fasullo, J. T. (2017). Atlantic meridional heat transports computed from balancing Earth's energy locally. *Geophysical Research Letters*, *44*(4), 1919–1927. https://doi.org/10.1002/2016GL072475

Van Wart, J., Grassini, P., Yang, H., Claessens, L., Jarvis, A., & Cassman, K. G. (2015). Creating long-term weather data from thin air for crop simulation modeling. *Agricultural and Forest Meteorology*, *208*, 49–58. https://doi.org/10.1016/j.agrformet.2015.02.020

Walker, J. C., Carboni, E., Dudhia, A., & Grainger, R. G. (2012). Improved detection of sulphur dioxide in volcanic plumes using satellite-based hyperspectral infrared measurements: Application to the Eyjafjallajökull 2010 eruption. *Journal of Geophysical Research*, *117*(D20), D00U16. https://doi.org/10.1029/2011JD016810

Wang, M., Hu, C., Barnes, B. B., Mitchum, G., Lapointe, B., & Montoya, J. P. (2019). The great Atlantic sargassum belt. *Science*, *365*(6448), 83–87. https://doi.org/10.1126/science.aaw7912

Wang, Y., & Zhang, G. J. (2016). Global climate impacts of stochastic deep convection parameterization in the NCARCAM5. *Journal of Advances in Modeling Earth Systems*, *8*(4), 1641–1656. https://doi.org/10.1002/2016MS000756

Warner, J. X., Dickerson, R. R., Wei, Z., Strow, L. L., Wang, Y., & Liang, Q. (2017). Increased atmospheric ammonia over the world's major agricultural areas detected from space. *Geophysical Research Letters*, *44*(6), 2875–2884. https://doi.org/10.1002/2016GL072305

Wielicki, B. A., Barkstrom, B. R., Harrison, E. F., Lee, R. B., III, Smith, G. L., & Cooper, J. E. (1996). Clouds and the Earth's radiant energy system (CERES): An Earth Observing System experiment. *Bulletin of the American Meteorological Society*, *77*(5), 853–868. https://doi.org/10.1175/1520-0477(1996)077<0853:catere>2.0.co;2

WMO (World Meteorological Organization). (2012). In *Proceedings of the 5th WMO workshop on the impacts of various observing systems on numerical weather prediction*. (p. 24). World Meteorological Organization.

Wong, S., & Teixeira, J. (2016). Extreme convection and tropical climate variability: Scaling of cold brightness temperatures to sea surface temperature. *Journal of Climate*, *29*(10), 3893–3905. https://doi.org/10.1175/jcli-d-15-0214.1

Worden, J. R., Kulawik, S. S., Fu, D., Payne, V. H., Lipton, A. E., Poloonsky, I., et al. (2019). Characterization and evaluation of AIRS-based estimates of the deuterium content of water vapor. *Atmospheric Measurement Techniques*, *12*(4), 2331–2339. https://doi.org/10.5194/amt-12-2331-2019

Xiong, X. X., & Barnes, W. (2006). An overview of MODIS radiometric calibration and characterization. *Advances in Atmospheric Sciences*, *23*(1), 69–79. https://doi.org/10.1007/s00376-006-0008-3

Yan, K., Li, H., Song, W., Tong, Y., Hao, D., Zeng, Y., et al. (2022). Extending a linear kernel-driven BRDF model to realistically simulate reflectance anisotropy over rugged terrain. *IEEE Transactions on Geoscience and Remote Sensing*, *60*, 1–16. https://doi.org/10.1109/TGRS.2021.3064018

Yao, Z., Hong, J., Cui, X., Zhao, Z., & Han, Z. (2022). A neural network based single footprint temperature retrieval for atmospheric infrared sounder measurements and its application to study on stratospheric gravity wave. *Journal of Tropical Meteorology*, *28*(1), 82–94. https://doi.org/10.46267/j.1006-8775.2022.007

Zhang, J., Mu, Q., & Huang, J. (2016). Assessing the remotely sensed drought severity index for agricultural drought monitoring and impact analysis in North China. *Ecological Indicators*, *63*, 296–309. https://doi.org/10.1016/j.ecolind.2015.11.062

Zhang, X., Liang, S., Wang, G., Yao, Y., Jiang, B., & Cheng, J. (2016). Evaluation of the reanalysis surface incident shortwave radiation products from NCEP, ECMWF, GSFC, and JMA using satellite and surface observations. *Remote Sensing*, *8*(3), 225. https://doi.org/10.3390/rs8030225

Zou, M., Xiong, X., Wu, Z., Li, S., Zhang, Y., & Chen, L. (2019). Increase of atmospheric methane observed from space-borne and ground-based measurements. *Remote Sensing*, *11*(8), 964. https://doi.org/10.3390/rs11080964